UCRL-JC-131429
PREPRINT

Simulations of Implosions with a 3D, Parallel, Unstructured-Grid, Radiation-Hydrodynamics Code

A. I. Shestakov, J. L. Milovich, T. B. Kaiser, M. K. Prasad

This paper was prepared for submittal to the
1998 Nuclear Explosives Development Conference
Las Vegas, NV
October 25-30, 1998

December 28, 1998

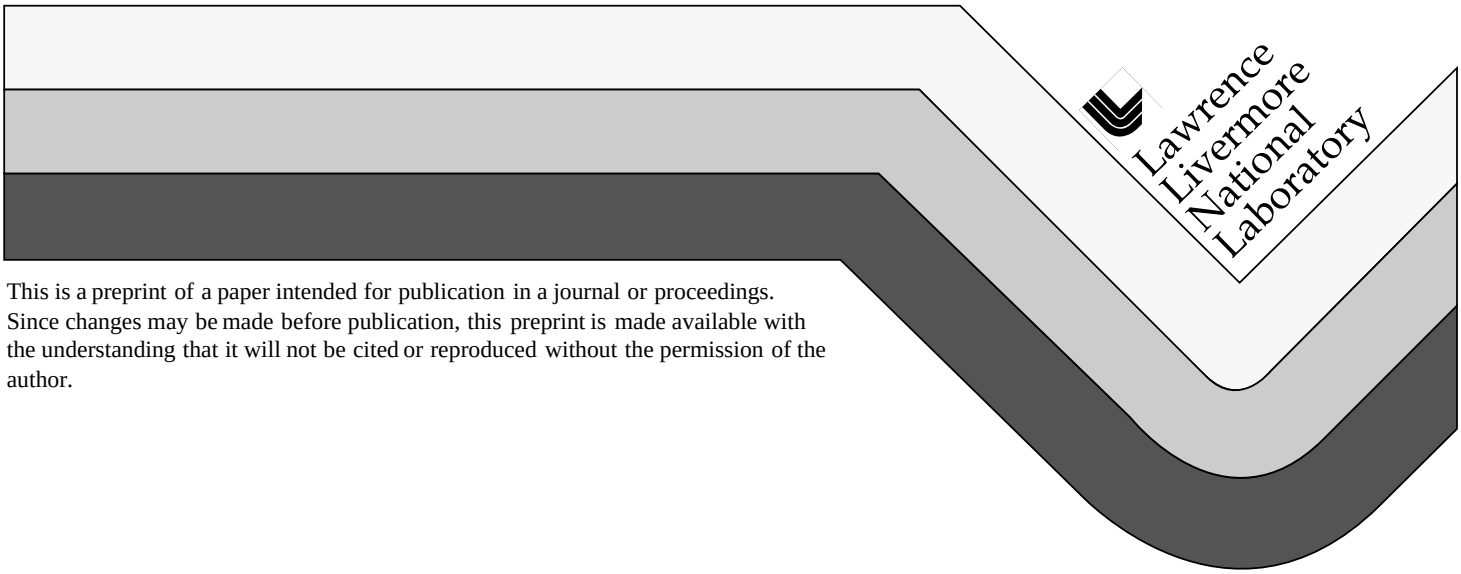

Simulations of Implosions with a 3D, Parallel, Unstructured-Grid, Radiation-Hydrodynamics Code [1]

A. I. Shestakov, J. L. Milovich, T. B. Kaiser, and M. K. Prasad
Lawrence Livermore National Laboratory
Livermore CA 94550

An unstructured-grid, radiation-hydrodynamics code is used to simulate implosions. Although most of the problems are spherically symmetric, they are run on 3D, unstructured grids in order to test the code's ability to maintain spherical symmetry of the converging waves. Three problems, of increasing complexity, are presented. In the first, a cold, spherical, ideal gas bubble is imploded by an enclosing high pressure source. For the second, we add non-linear heat conduction and drive the implosion with twelve laser beams centered on the vertices of an icosahedron. In the third problem, a NIF capsule is driven with a Planckian radiation source.

Keywords: hydrodynamics, heat conduction, radiation transport, parallel codes

Introduction

This paper presents results obtained with ICF3D, a 3D, parallel, unstructured grid, finite element, radiation-hydrodynamic-diffusion code [1] which contains the following physics modules:

- Real material equation-of-state (EOS) using the SESAME tabular data [2]
- Compressible hydrodynamics
- Laser energy deposition
- Heat conduction (diffusion of matter temperature T)
- Radiation transport (diffusion of radiation energy density E_r)

In ICF3D, the unstructured grid consists of an arbitrary collection of cells (tetrahedra, pyramids, prisms, and/or hexahedra), with the only restriction that cells share like-kind faces. ICF3D may be run in any of three coordinate systems: Cartesian, cylindrical, or spherical. The code combines cell-centered methods (for hydrodynamics) with point-centered methods (for diffusion). The ALE hydrodynamic scheme is discretized using discontinuous finite elements [3] while continuous finite elements discretize the diffusion packages. The code is written in the object oriented language C++ and is portable; it runs on uniprocessors or on parallel machines. ICF3D parallelizes by decomposing physical space into a collection of subdomains, one per processor [4].

In this paper we only present results. We are preparing another paper describing the numerical techniques. Interested readers are advised to contact the first author. Details on the laser energy deposition algorithm appear in Kaiser et al [5].

In the following sections we simulate three problems which test the code's ability to maintain spherical symmetry of converging waves and restrict attention to implosions. (Results for diverging

[1]Work performed under the auspices of the U.S. Department of Energy by the Lawrence Livermore National Laboratory under contract number W-7405-ENG-48.

waves, e.g., explosions, have been presented in [4].) The 3D results are obtained on unstructured tetrahedral grids generated by the LaGriT code [6] and the calculations are done using Cartesian coordinates. After generating the grid the METIS package [7] decomposes the domain to enable running in parallel. Since the problems are nearly spherically symmetric, we compare results to ICF3D "1D" simulations done using spherical coordinates with one cell in each of the angular directions.

The problems are presented in increasing order of complexity. The first two problems use an ideal gas EOS in which the pressure p, density ρ, internal energy e, and temperature T are related using the constants γ and $c_{\rm v}$,

$$p = (\gamma - 1)\,\rho e = (\gamma - 1)\,\rho\, c_{\rm v}\, T \ .$$

The first problem exercises only the hydrodynamic module. In the second, we couple laser energy deposition, heat conduction, and hydrodynamics. In the third, we simulate the indirect drive of a NIF capsule and use real materials (Beryllium and Deuterium), hydrodynamics, heat conduction, and radiation transport.

Ideal Gas Implosion

In this section we simulate the implosion resulting when a cold, quiescent, spherical gas bubble, initially of radius

$$r_0 = 1.0$$

is subjected to a boundary pressure of magnitude

$$p_b = 4/3$$

The gas EOS is specified using,

$$\gamma = 5/3$$

The initial conditions are,

$$\rho_0 = 1 \quad \text{and} \quad p_0 = \mathbf{v}_0 = 0$$

In this problem the gas motion is governed only by hydrodynamics. The conditions mimic those describing the Saltzman piston problem. Initially, the solution is similar to one with slab symmetry. Hence, the boundary pressure drives a shock into the gas which at first moves with speed

$$\dot{r}_s \approx -4/3$$

Since the shock is of infinite strength, behind the shock,

$$\rho = \frac{\gamma + 1}{\gamma + 1}\,\rho_0 \quad \text{and} \quad \mathrm{v}_r = -1$$

If the problem stayed slab-symmetric, the shock would traverse a unit distance in a time of 0.75 secs. However, because of the converging geometry, at $t \approx 0.57$, the shock reflects off the origin. In Fig. 1 we display ρ at $t = 0.56$, 0.58, and 0.6 for a finely meshed 1D run and also display ρ at

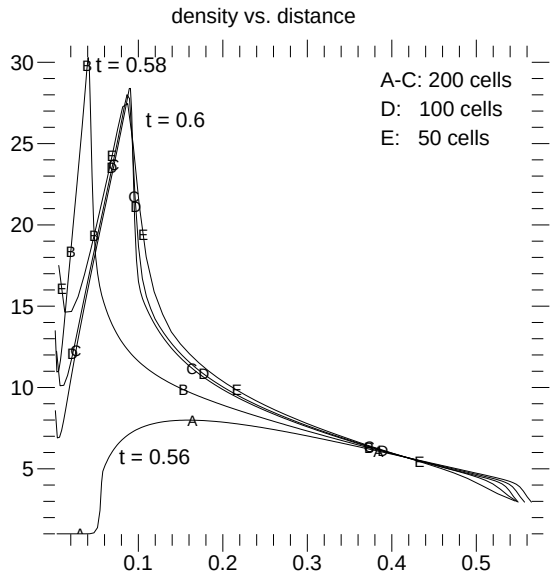

Figure 1: Ideal gas implosion; ρ vs. r. Lagrangian, 1D simulations with initially uniform cell widths. Curves A, B, and C are at $t = 0.56$, 0.58, and 0.6 resp. and use 200 cells. Curves D and E are at $t = 0.6$ and use 100 and 50 cells resp.

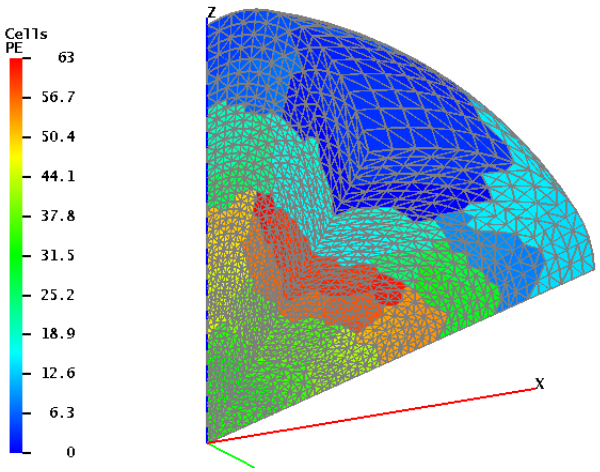

Figure 2: 3D Domain of ideal gas implosion problem. Shading designates PE numbers. Grid consists of 28,208 tetrahedra (50 radial cells), 5791 points, and 58,455 faces.

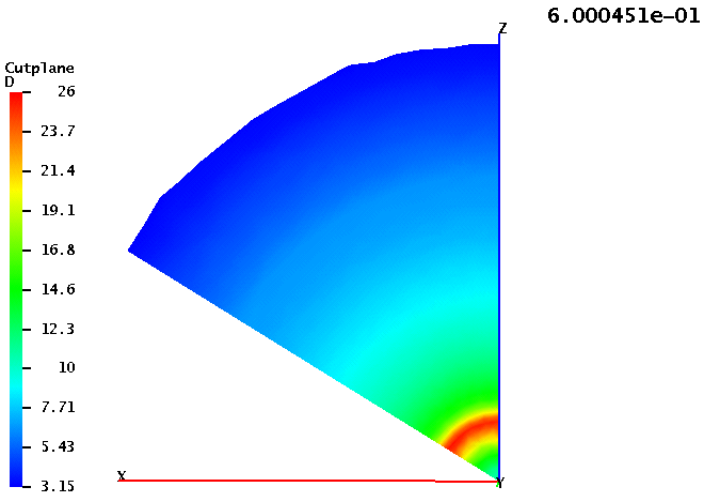

Figure 3: Ideal gas implosion; side-on view of density; $t = 0.6$ sec; $\max(Z) = 0.563$

$t = 0.6$ for two coarser discretizations. Results show that the coarsest mesh (50 cells) suffices to obtain relatively good accuracy, especially if we compare the shock's position.

The 3D simulation is run on an unstructured grid discretizing the icosahedral wedge depicted in Fig. 2 in which the shading corresponds to the PE number. The initial domain is bounded by the sphere of radius r_0, the two azimuthal planes: $\phi = \pm\pi/5$, and the plane intersecting the origin and the points: $(\theta, \phi) = (\theta_0, \pm\pi/5)$ where

$$\cos\theta_0 = 1/\sqrt{5} \tag{1}$$

The simulation was done on 64 PEs of the LLNL IBM SP2 and ran until $t = 0.9$ at which time the reflected shock had interacted with the incoming wall. Figure 3 displays a side-on view of ρ at $t = 0.6$

A comparison between Figs. 1 and 3 shows that $\max(Z)$ and the shock position are very similar and the $\min(\rho)$ also agree while the $\max(\rho)$ are within 6% of each other since in the 1D result with 50 cells, $\max(\rho) = 27.46$ Lastly, Fig. 3 shows the code's ability to maintain spherical symmetry, despite running on the asymmetric tetrahedral grid.

Laser Driven Implosion

Here we simulate the implosion of a quiescent, spherical gas bubble, initially of radius

$$r_0 = 0.2$$

In this problem we use the hydrodynamic, heat conduction, laser packages, and an ideal gas EOS in which,

$$\gamma = 1.4 \quad \text{and} \quad c_v = 10^{15}\,\text{erg}\,(\text{gm keV})^{-1}\ .$$

In the heat conduction package, the flux $\mathcal{H} = -\chi\nabla T$, is in units of erg/(cm^2 sec). For the simulation we model non-linear heat conduction by setting

$$\chi = \chi_0 T^{5/2} \quad \text{and} \quad \chi_0 = 10^{11}$$

The traversal of laser rays through the gas and the subsequent energy deposition depends on the free electron number density n_e (cm^{-3}). Laser rays cannot propagate in regions where n_e is larger than the the critical number density

$$n_c = \pi m_e (f_\ell / e)^2 \ \ (\mathrm{cm}^{-3})$$

where m_e is the electron mass, e is the electron charge, and $f_\ell = 2.866 \cdot 10^{14}$ sec^{-1} is the chosen frequency of the laser. The critical density n_c is used to compute the critical mass density ρ_c. For simplicity, we assume the gas to be fully ionized hydrogen. Hence, if $\mathcal{A}$ is the Avogadro number, $\rho_c = n_c / \mathcal{A}$ and we obtain,

$$\rho_c \approx 1.668 \cdot 10^{-3} \ \mathrm{gm\,cm}^{-3} \ .$$

In order to allow the laser to enter the gas and deposit its energy only at the surface, the gas is initialized to be largely over-dense using the following point centered distribution:

$$\rho|_{t=0} = \begin{cases} 10 \times \rho_c & \text{if } r \le r_0 - 2\Delta \\ 2 \times \rho_c & \text{if } r = r_0 - \Delta \\ 0.01 \times \rho_c & \text{if } r = r_0 \end{cases}$$

where $\Delta = r_0/16$. We simulate a "cold" start by setting,

$$T|_{t=0} = 1 \ \mathrm{eV}.$$

These conditions imply that the initial energy of the bubble is, $E_0 \approx 4.35 \cdot 10^8$ erg. However, in the 3D simulation, because of discretization errors, we obtain

$$E_0 \approx 4.20 \cdot 10^8 \ \mathrm{erg}.$$

The physics packages require boundary conditions. For the heat conduction package, symmetry is imposed at the boundary. For the hydrodynamics, we set

$$p = p_b = 6.67 \cdot 10^7 \ \mathrm{erg\,cm}^{-3} \ .$$

Since the average density in the outer shell: $r_0 - \Delta \le r \le r_0$ is approximately ρ_c , p_b is 10 times less than the average pressure in the outer shell. This lets the outer shell expand which allows more rays to enter the problem and deposit their energy.

For this problem, the laser package simulates twelve beams, each of circular X-section of radius equal to r_0 and each of equal intensity. The beams are centered on the vertices of a regular icosahedron, which in the $\theta < \pi/2$ hemisphere lie at $\theta = 0$ and $(\theta, \phi) = (\theta_0, 2\pi j/5)$ where $j = 0, 1, \ldots 4$ and θ_0 is defined in Eq. 1. Each beam's intensity is $2.875 \cdot 10^{13}$ W cm^{-2}.

We simulate a "flat top" temporal power deposition profile. The laser is turned on at $t = 0$ and turned off at $t = 2$ nsec. Multiplying the total beam intensity by 2 nsec gives $8.67 \cdot 10^{11}$ erg, the maximum energy that the laser can deliver. However, because the capsule is largely over dense, initially, most of the laser rays reflect and very little energy is deposited. After 2 nsec, only

$$E_\ell = 8.39 \cdot 10^{10} \ \mathrm{erg}$$

is absorbed by the gas. This is approx. 10% of the laser energy, but is still nearly 200 times E_0.

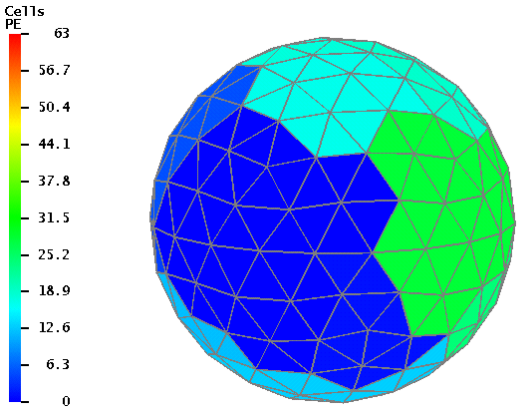

Figure 4: Computational mesh of laser driven implosion problem. Grid consists of 11,580 tetrahedra (16 radial cells), 2053 points, and 23,320 faces.

The laser's energy, deposited on the outermost cells, is a source for the heat conduction package. This drives a thermal wave inward which quickly slows down and the resulting pressure gradient forms the imploding shock.

The simulation is run on the domain depicted in Fig. 4 in which the shading depicts the domain decomposition of a prior simulation for 64 PEs. The present simulation uses only 16 PEs. In Fig. 5, we display ρ across the $X = 0$ plane at $t = 12$ nsec, a time shortly after the shock reflects off the origin. Note that $\max(\rho)$ is nearly 50 times its initial value. The figure displays only the central part of the domain. After $t = 12$ nsec, the reflected shock continues moving outward. We end the simulation at $t = 16$ nsec and display the final density in Fig. 6. As in Fig. 5, only the central part of the domain is displayed. The hollow ρ profile behind the shock is similar to that displayed in Fig. 1.

We conclude this section by noting how well the solution maintains symmetry and stress that Figs. 5 and 6 display ρ across a plane cutting through the 3D problem domain.

ICF Capsule Implosion

For the third problem, we simulate the implosion of an ICF capsule consisting of a nearly vacuous inner region enclosed by two spherical shells. The capsule dimensions, materials and initial densities are given in the following table.

Dimensions (cm)	Material	Density (g cm^{-3})
$r \le r_g = 0.1$	Deuterium	10^{-3}
$r_g \le r \le r_f = 0.11$	Deuterium	0.21
$r_f \le r \le r_a = 0.121$	Beryllium	1.85

The material EOSs are given by the LANL SESAME tables [2]. Since the tables do not have data at low temperatures, we initialize with $T = 7$ eV.

In this problem, we use the hydrodynamic, heat conduction, and radiation transport packages. In the heat conduction module, the conductivity is given by the Lee & More formulae [8, 9] with modifications suggested by G. Zimmerman [10]. Radiation transport is approximated by a diffusion equation for the radiation energy density E_r which is coupled to the matter energy equation.

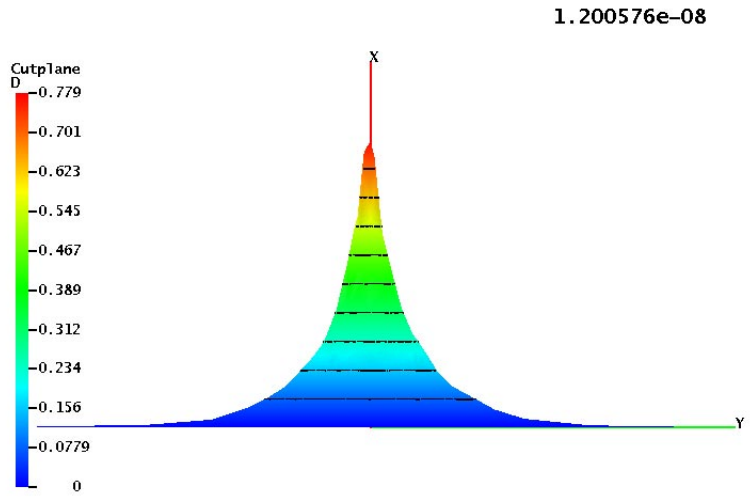

Figure 5: Laser driven implosion problem. Density ρ across the $X = 0$ plane, $t = 1.2 \cdot 10^{-8}$ sec.

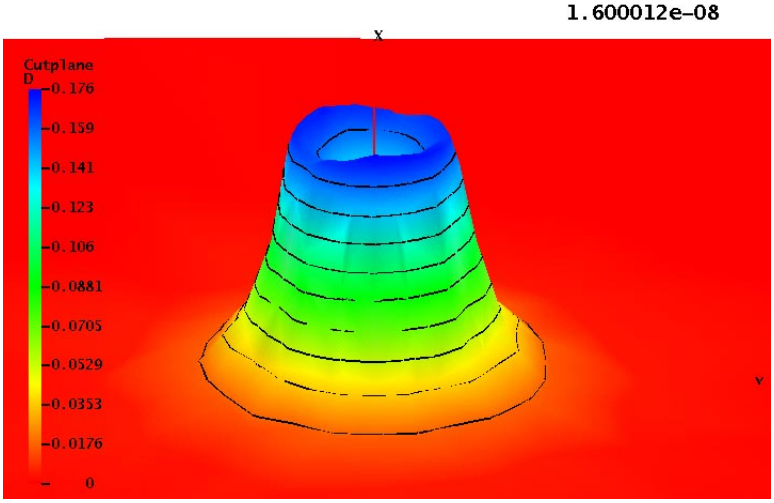

Figure 6: Laser driven implosion problem. Density ρ across the $X = 0$ plane, $t = 1.6 \cdot 10^{-8}$ sec.

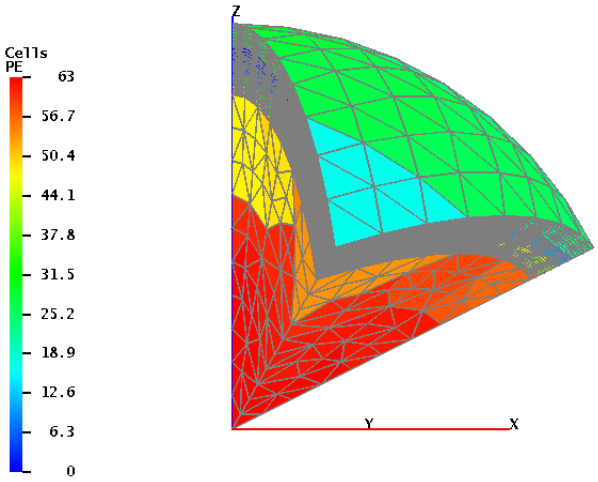

Figure 7: 3D Domain of ICF capsule implosion problem. Shading designates PE numbers. Grid consists of 5,104 tetrahedra, 1246 points, and 10,915 faces; radial discretization uses 10 cells in the gas, 12 cells for the fuel, and 11 for the ablator.

We use Rosseland averaged opacities to define the diffusion coefficient and Planck averaged opacities for the coupling coefficient.

As boundary conditions, for the hydrodynamics, we set $p = 58.22$ GPa on the surface of the capsule. This corresponds to the pressure of Be at $\rho = 1.85$ and $T = 1$ eV. For the heat conduction package, a symmetry condition is imposed, and for the radiation we set

$$E_r - (2/c)\, F_r \cdot \hat{n} = E_s \tag{2}$$

where F_r is the radiative flux, $\hat{n}$ is the outward unit normal, and E_s is set in accordance to a radiation temperature $T_r = 0.16$ keV. The boundary conditions are always on and simulate a capsule inside a hohlraum kept at constant T_r.

For the simulation, we run on an unstructured tetrahedral grid which discretizes an icosahedral wedge. The initial mesh is displayed in Fig. 7

The simulation consists of a typical (albeit not well tuned) indirectly driven implosion. Equation 2 deposits energy on the ablator surface which heats up, expands and creates an imploding shock. The shock first traverses the ablator, then the fuel, and later the gas. At both interfaces, $r = r_f$ and $r = r_g$ the shock travels from a high density region to one of lower density, a scenario for a possible Richtmyer-Meshkov instability. In the ablator, the radiation source is delivered to a thinning and moving spherical surface, a condition ripe for Rayleigh-Taylor instabilities as the tenuous hot region pushes on the denser shocked ablator. In Figs. 8, 9, and 10 we present side-on views of ρ, T, and the radiation temperature T_r at $t = 8$ nsec when the imploding shock has reflected off the origin; only the central region is displayed. The figures are characteristic of a capsule implosion. The thin, imploding shell is evident in Fig. 8 which highlights the high density region. Figure 9 shows that $T = 0.716$ keV near the origin. Outside the central region, out to the ablation front, T is relatively cold. Beyond the ablation front, $T \approx 158$ eV due to its coupling to T_r. In Fig. 10 we see the ablation front, outside of which $T_r = 158$ eV. Inside the front, T_r is

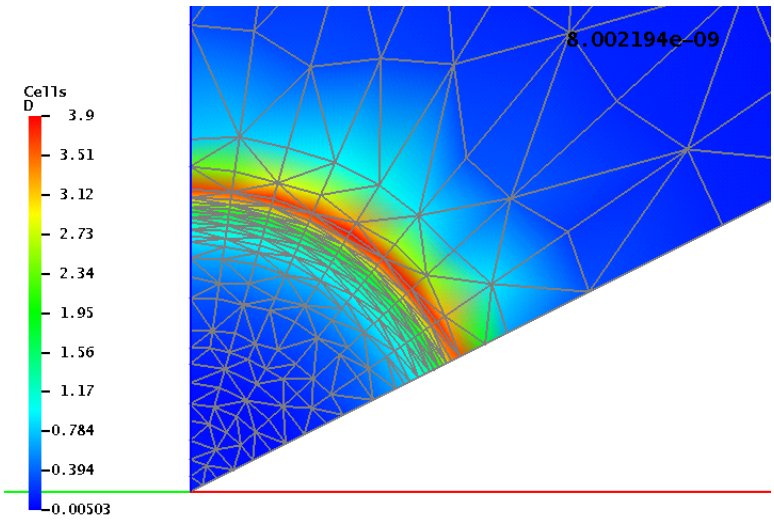

Figure 8: ICF capsule implosion; side-on view of density; $t = 8 \cdot 10^{-9}$ sec.

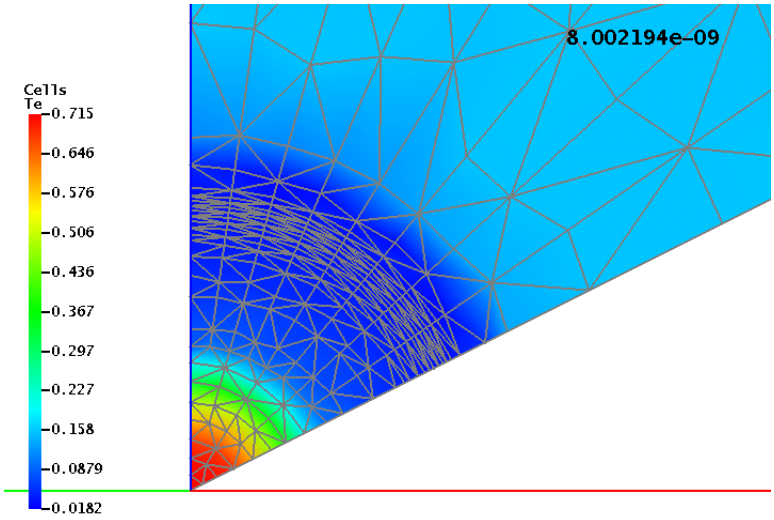

Figure 9: ICF capsule implosion; side-on view of matter temperature; $t = 8 \cdot 10^{-9}$ sec.

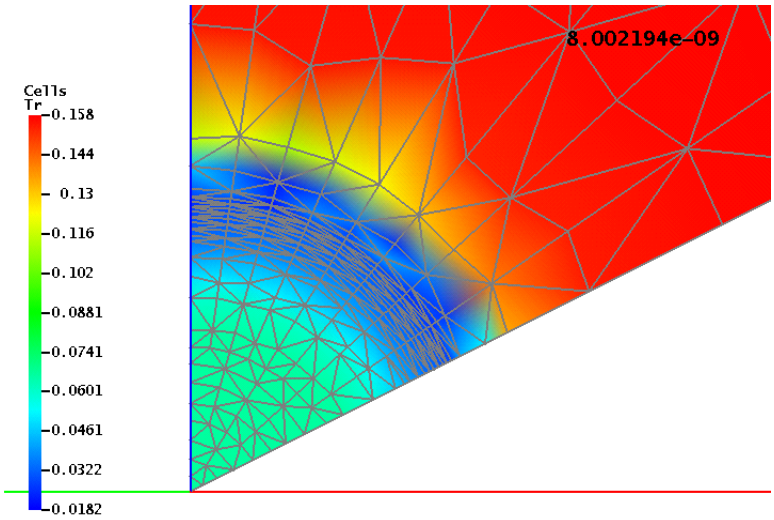

Figure 10: ICF capsule implosion; side-on view of radiation temperature; $t = 8 \cdot 10^{-9}$ sec.

relatively cold, approx. 18 to 30 eV, while in the central region $T_r \approx 75$ eV due to its coupling to T. All three figures clearly display the near spherical symmetry of the implosion.

In order to compare with a 1D run, in Fig. 11 we display results at $t = 10$ nsec using slightly finer zoning. For this run, $t = 10$ nsec is nearly the time of peak compression. Figure 11 shows that T and T_r (curves C and D) are tightly coupled except in the central region where T has increased to 0.8 keV. Curve E shows that there is still a lot of kinetic energy in the implosion; in the region $0.015 < r < 0.02$ cm, the velocity ranges between -2 and $-4 \cdot 10^8$ cm sec^{-1}. Finally, curve F is the Be mass fraction, initially a step function centered at $r = r_f = 0.11$ cm.

Summary and Discussion

We have presented results of hydrodynamic implosions on test problems relevant to ICF. The problems were run with ICF3D, a 3D unstructured grid code on 3D, unstructured tetrahedral grids. Except for problem #2, the problems are inherently spherically symmetric, but were run in 3D in order to test the code's ability to maintain spherical symmetry. In problem #2, which simulates an idealized directly driven ICF capsule, we also obtained symmetry.

We are, of course, pleased with the results and admit to being pleasantly surprised. Problems #1 and #3 were run in the Lagrangian mode with no intervention to keep the mesh from tangling, except that on symmetry planes, e.g., at $\phi = \pm\pi/5$, the points were constrained to stay on the planes. In problem #2, because the laser beams might cause the exterior points to expand asymmetrically, we used the code's ALE option and restricted the mesh points to only move radially. We note that computing on unstructured grids seems to bring two advantages. First, with such grids, one may easily add cells where needed and use fewer elsewhere, e.g., by refining in the transverse direction with increasing radius. Second, problems seem to run better on such grids. For example, we also ran problem #2 on a logically orthogonal grid obtained by discretizing a sphere with constant polar and azimuthal angles. Such a grid adds a long wavelength asymmetry to the mesh and waves can travel at different speeds along the pole and the equatorial plane. This asymmetry then causes premature mesh tangling. For example, problem #2 when run on such a grid, halted at 10

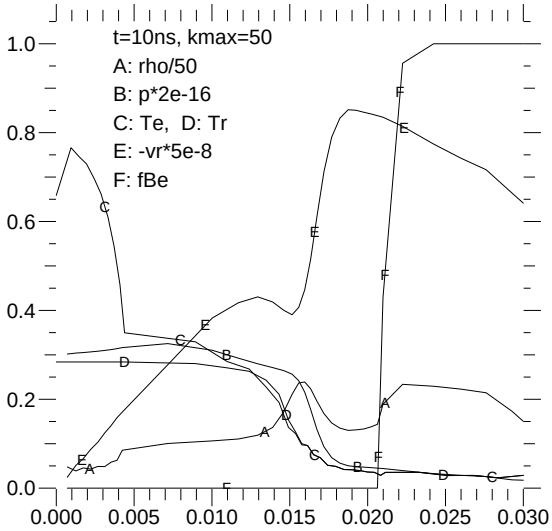

Figure 11: ICF capsule implosion, 1D run. Units: ρ in g cm^{-3}, p in erg cm^{-3}, T and T_r in keV, v in cm sec^{-1}, and curve E is the Be mass fraction; $t = 10^{-8}$ sec.

or 11 nsec, before the shock hit the origin.

Acknowledgement

The ICF3D code was initiated by D. S. Kershaw, M. K. Prasad, and M. Shaw who set out to write a 3D hydrodynamic code using discontinuous finite elements in the C++ computer language. Along the way ICF3D has benefited from the contributions of many individuals. We especially thank G. B. Zimmerman for very useful technical support. We also thank D. George and the entire LaGriT code group of the LANL for supplying the ability to generate unstructured grids. Regrettably, the ICF3D code project has been canceled in favor of the KULL effort whose progress is described in these proceedings by D. Miller et al.

References

[1] A. I. Shestakov, M. K. Prasad, J. L. Milovich, N. A. Gentile, J. F. Painter, and G. Furnish, "The ICF3D Code," Lawrence Livermore National Laboratory, Livermore, CA, UCRL-JC-124448, (1997), submitted to *Comput. Methods Appl. Mech. Engin.*

[2] "SESAME: The Los Alamos National Laboratory Equation of State Database," Eds. S. P. Lyon and J. D. Johnson, Los Alamos National Laboratory Report LA-UR-92-3407. Also: "T-1 Handbook of Material Properties Data Bases," K. S. Holian, Ed., Los Alamos National Laboratory Report LA-10160-MS Nov 1984.

[3] D. S. Kershaw, M. K. Prasad, M. J. Shaw, and J. L. Milovich, *Comput. Methods Appl. Mech. Engin.*, **158** (1998) 81-116.

[4] A. I. Shestakov and J. L. Milovich "Parallelization of an Unstructured Grid, Hydrodynamic-Diffusion Code," in *Solving Irregularly Structured Problems in Parallel*, 5th International

Symposium, IRREGULAR'98 Berk., Ca., USA, Aug. 9-11, 1998 Proceedings, A. Ferreira, J. Rolim, H. Simon, S.-H. Teng (Eds.) Lecture Notes in Computer Science 1457, Springer.

[5] T. B. Kaiser, J. L. Milovich, A. I. Shestakov, and M. K. Prasad, "A New Laser Driver for Physics Modeling Codes using Unstructured 3D Grids," in these proceedings.

[6] www.t12.lanl.gov/ lagrit

[7] G. Karypis and V. Kumar, "A fast and high quality multilevel scheme for partitioning irregular graphs," Technical Report TR 95-035, Department of Computer Science, Univ. Minn., 1995. To appear in *SIAM Journal on Scientific Computing 1997*. A short version appears in Intl. Conf. on Parallel Processing 1995. The METIS program is available on the web from: http://www-users.cs.umn.edu/ karypis/metis/metis/ main.html

[8] R. M. More, "Atomic Physics of Laser-Produced Plasmas," *Handbook of Plasma Physics*, Eds. Rosenbluth and Sagdeev, Vol. 3: *Physics of Laser Plasma*, Eds. Rubenchik and Witkowski, Elsevier Science Pubs. B. V., 1991, Ch. 2, p. 63.

[9] Y. T. Lee and R. M. More, *Phys. Fluids* **27** 5, May 1984, p. 1273.

[10] G. B. Zimmerman, private communication, Lawrence Livermore Natl. Lab. (1998).